Molecular packing analysis of the crystal smectic E phase of a benzothieno-benzothiophene derivative by a combined experimental / computational approach

Sebastian Hofer, Wolfgang Bodlos, Jiří Novák, Alessandro Sanzone, Luca Beverina & Roland Resel

View supplementary material ☑

Published online: 04 May 2021.

Submit your article to this journal ☑

Article views: 258

View related articles ☑

View Crossmark data ☑

Molecular packing analysis of the crystal smectic E phase of a benzothieno-benzothiophene derivative by a combined experimental / computational approach

Sebastian Hofer [a], Wolfgang Bodlos [a], Jiří Novák [b], Alessandro Sanzone[c], Luca Beverina [c] and Roland Resel [a]

aInstitute of Solid State Physics, Graz University of Technology, Graz, Austria; bDepartment of Condensed Matter Physics, Masaryk University, Brno, Czech Republic; cDepartment of Materials Science, University of Milano-Bicocca, Milano, Italy

ABSTRACT

The molecule 2-decyl-7-phenyl[1]benzothieno[3,2-b][1]benzothiophene has gained a lot of attention since high charge carrier mobility was observed in thin film transistors. Its thermotropic liquid crystalline states may play an important role in the thin film formation since the *smectic A* and the *crystal smectic E* phase (SmE) are claimed to be pre-stages of the final bulk structure. To understand the phase diversity, structural characterisation of solution processed thin films is performed by X-ray diffraction in the complete temperature range up to the isotropic state at 240°C. The diffraction pattern of the SmE phase is analysed in detail. Peak broadening analysis reveals that the crystal-lographic order across the smectic layers is larger than the order along the smectic layers. A combined experimental and computational approach is used to determine the molecular packing within the SmE phase. It leads to a number of different packing motifs. A comparison of the calculated diffraction pattern with the experimental results reveals that nano-segregation is present within the SmE phase. Energy consideration clearly favours a herringbone arrangement of the aromatic units. The nano-segregation within the SmE phase with herringbone packing of the aromatic units is accompanied with interdigitation of side chains from neighbouringherringbone layers.
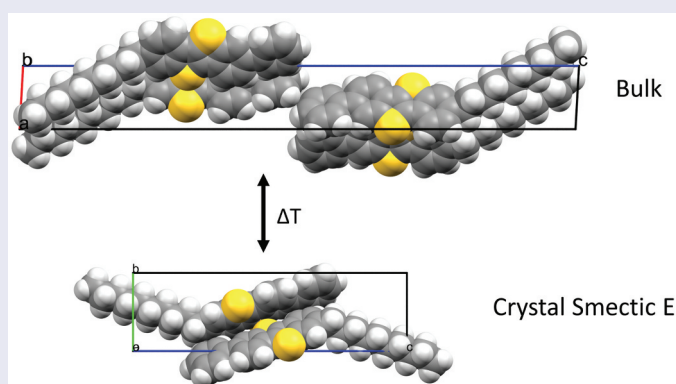
Introduction

The class of alkyl substituted benzothienobenzothiophene-type molecules gained considerable attention due to high charge carrier mobilities in organic thin film transistors. Values of up to 9 cm^{2}V^{-1}s^{-1} are observed [1,2]. The presence of alkyl chains symmetrically attached at the terminal ends of the molecule provides overall flexibility in device fabrication since thin films can be prepared by solution processing [3,4] as well as by physical vapour deposition [5,6]. Moreover, the thermotropic

liquid crystalline state can be used in the thin film preparation procedure to obtain a defined structure within thin films [7,8].

Recently, a new asymmetric derivative of BTBT – the molecule 2-decyl-7-phenyl[1]benzothieno[3,2-b][1] benzothiophene (Ph-BTBT-10) – was introduced [9]. The asymmetry in the substitution pattern, featuring a phenyl residue on the 2-position of the BTBT core and a decyl chain on the 7-position, results in a more diverse phase behaviour [10]. Liquid crystalline states with high structural order appear. It is reported that

these states can be used as pre-stages of the final bulk crystallisation so that crystals with extended size can be prepared within thin films [11].

The asymmetry of the molecule causes crystallisation with a bilayer herringbone structure [9,10]. The structure is formed by stacked individual layers consisting of aromatic units arranged in a herringbone manner and decyl chains formed by the terminal alkyls. Two herringbone layers stack directly on top of each other leading to double herringbone layers. The crystal structure can be described by a sequence of these double herringbone layers followed by double layers of the decyl chains. The lattice constants of the structure are a = 6.047 Å, b = 7.757 Å, c = 53.12 Å and β = 93.14° whereby c spans over two herringbone layers and two alkyl layers [12]. In summary, the molecules show a *head-to-head* arrangement (along the c-axis) since the aromatic units of molecules from neighbouring herringbone layers are antiparallel to each other. A phase transition to *smectic E* (SmE) with a *head-to-tail* arrangement of the molecules is observed at temperatures around 144°C [9,10]. The presence of a SmE phase was concluded by polarised optical microscopy investigations [13]. Analysis of the molecular packing at elevated temperatures is already performed by molecular dynamics simulations, suggesting a structure built by stacked single-molecular sheets in a *head-to-tail* arrangement. However, the arrangement of the molecules within the SmE phase is still not clear [14–16].

Recent developments in the field of crystal structure solution from thin films allow the determination of the molecular packing within unknown crystal structures exclusively present within thin films [17,18]. Grazing incidence X-ray diffraction (GIXD) in combination with specular X-ray diffraction (XRD) is used for this purpose. Despite the limited information of only a few diffraction peaks, a combination of experimental performance and theoretical calculations can be suitable to determine the molecular packing [19]. Here, we will apply our knowledge on the crystal structure solution from thin film to the SmE phase of the molecule Ph-BTBT-10.

Experimental

Thin film preparation

The molecule Ph-BTBT-10 was synthesised according to the strategy shown in Scheme 1 that some of us recently published [20]. The commercially available [1]benzothieno[3,2-b][1]benzothiophene (BTBT) core was regioselectively acylated at the 2 position via a Friedel Crafts reaction with decanoyl chloride. The obtained ketone was converted to 2-decyl-[1]benzothieno[3,2-b][1]benzothiophene (C10-BTBT) through reduction with

a $NaBH_4/AlCl_3$ mixture in good yield. Bromination of the latter with bromine in chloroform afforded 2-decyl-7-bromo-[1]benzothieno[3,2-b][1]benzo-thiophene (Br-BTBT-10) after chromatographic purification. Finally, a Suzuki–Miyaura coupling between Br-BTBT-10 and phenyl boronic acid in a Kolliphore EL 2 wt%: toluene emulsion (9:1 v/v) in the presence of triethyl amine as the base and [1,1′-Bis(di-tert-butylphosphino)ferrocene] dichloropalladium(II) Pd(dtbpf)Cl$_2$ as the catalyst gave 10-BTBT-Ph in essentially quantitative yield.

Thin film samples were prepared via spin-coating or drop-casting from toluene solutions of varying concentrations and spin speeds (0.2 up to 5.0 g/l and 500 up to 3000 rpm) onto thermally oxidised silicon wafers. Powder samples were prepared by transferring a small amount of about 1 mg of polycrystalline material onto a silicon substrate and a subsequent flattening procedure.

Analytical methods

Specular XRD was carried out with a PANalytical Empyrean diffractometer in θ-θ geometry using CuK$_\alpha$ radiation. On the incident side a parallel beam X-ray mirror was used for monochromatisation and collimation. At the diffracted beam path, an anti-scatter slit as well as a 0.02 rad Soller slit was used together with a PIXcel3D detector operating in either receiving 0D-mode or scanning 1D mode. Temperature-dependent in situ measurements were performed with a DHS 900 heating stage from Anton Paar Ltd. Graz [21]. The experiments were performed under nitrogen atmosphere. The data are converted into reciprocal space by $q = \frac{4\pi}{\lambda}\sin\left(\frac{2\theta}{2}\right) = \frac{2\pi}{d_{hkl}}$ with λ as the wavelength of the primary X-ray beam, 2θ the scattering angle and d_{hkl} the interplanar distance of the (hkl) plane. In case of a specular scan, the total length of the scattering vector q has a contribution only in z-direction (perpendicular to the substrate surface).

Grazing incidence X-ray diffraction (GIXD) at ambient temperatures was carried out at the beamline XRD1 at Elettra Synchrotron Trieste with a radiation wavelength of 1.4 Å using an incidence angle of α$_i$ = 0.8° on a goniometer in kappa geometry [22]. A PILATUS 2 M detector was used to collect diffracted intensity. To improve statistics, the sample was rotated during measurement and six images with an exposure time of 30 s each were collected during one full sample rotation. Temperature-dependent in situ GIXD was performed using a Rigaku SmartLab 9 kW equipped with a Cu rotating anode, collimating parabolic multilayer mirror and pinhole optics. A HyPix 3000 2D detector was utilised for collecting GIXD measurements. Because of low signal, a series of 40 images was measured for 1 h each and summed up to improve the

signal-to-noise ratio. A DHS 1100 commercial high-temperature stage from Anton Paar, covered by a carbon dome and filled with a nitrogen atmosphere, was used during heating [23].

Data from GIXD are presented as reciprocal space maps with the out-of-plane (q_z) and in-plane component (q_{xy}) of the scattering vector q as an orthogonal basis, with the q_z component parallel to the surface normal and the q_x / q_y plane parallel to the substrate surface. The scattering vector components are determined for each detector pixel from the incident angle α_i and the outgoing angle α_f in the sample coordinate system and from a calibration measurement on an LaB$_6$ film, to determine additional parameters, e.g. the distance from the sample to the detector. Resulting data was evaluated with the use of the in-house developed software package GIDVis [24]. The resulting reciprocal space maps are corrected based on geometrical correction factors, i.e. Lorentz and polarisation factors.

For analysing the films in terms of paracrystallinity, the peaks were fitted with a Gaussian function in both in-plane (q_{xy}) and out-of-plane (q_z) directions. For the resulting peak widths Δq_{xy} and Δq_z a linear regression based on $(\Delta q)^2 = 4 \left[\left(\frac{\pi}{D_{hkl}} \right)^2 + \left(\frac{\pi^3 g^2 m^2}{d_{hkl}} \right)^2 \right]$ is calculated, where m and d_{hkl} denote the order of the diffraction peak in terms of its Laue index (h, k or l) and the inter-planar spacing of the diffraction peaks, respectively. This allows determining the crystallite size D_{hkl} and the amount of paracrystallinity g of the sample in two individual directions. No correction for the instrumental peak broadening was used.

Computational method

Determination of the molecular packing within the SmE phase was performed by an experimental/computational approach. In the first step, the lattice constants were determined by indexing of the GIXD pattern. The crystallographic unit cell was used as an input for molecular dynamics (MD) simulation revealing the molecular packing. These simulations were carried out with the LAMMPS software package [25] using the CHARMM general force field version 3.0.1 [26]. Several thousand trial structures are generated by placing two randomly oriented molecules in an expanded (120%) unit cell. During the simulation run, the starting configuration was relaxed and reduced to the experimentally determined unit cell size. The resulting structures are then clustered based on similarities of the packing motifs. Each selected packing motif appeared multiple times at the respective total energy. The obtained packing motifs are judged by a comparison of observed (F_{obs}) and

calculated structure factors (F_{calc}) taken from the diffraction intensities on the basis of a reliability factor $R = \frac{\sum ||F_{obs}| - |F_{calc}||}{\sum |F_{obs}|}$.

Experimental results

A series of specular XRD measurements were performed on a spin-coated (5 g/l, 3000 rpm) film in the temperature range from room temperature up to 240°C. Figure 1(a) shows XRD scans at selected temperatures. At room temperature (25°C), a dominant peak series at $q_z = (0.118 * l) \, \mathring{A}^{-1}$ (with l as the Laue index) is observed which can be assigned to the $00l$ diffraction peaks of the bulk crystal phase of the molecule Ph-BTBT-10 [12]. The interplanar distance of the 001 plane at 52.3 Å clearly reflects the bilayer structure of the known bulk phase. The absence of hkl reflections with $h \neq 0$ or $k \neq 0$ reveals a strong preferred orientation of the crystallites with the (001) plane parallel to the substrates surface. At a temperature of 149°C, the peak sequence changes to $q_z = (0.216 * l) \, \mathring{A}^{-1}$ which corresponds to the characteristic $00l$ peak series of the SmE phase with an interplanar distance of 29.1 Å of the (001) plane. With increasing temperature up to 215°C, the peak position gradually shifts to lower q_z values due to thermal expansion. A sudden shift in the peak positions as well as in the peak intensities is observed at 220°C. This peak series is observed at $q_z = (0.223 * l) \, \mathring{A}^{-1}$ corresponding to an interplanar distance of 28.1 Å and is assigned to the *smectic A* (SmA) phase [9,13]. At 240°C, the diffraction peaks disappear which is assigned to a transition to the isotropic state. Figure 1(b) shows a waterfall plot of the specular diffraction pattern in the temperature range from 130 to 240°C. Each scan was measured for 10 min at a fixed temperature which was increased in steps of 2°C in the vicinity of the phase transition temperature and in steps of 10°C at more remote temperature ranges. The phase transition temperatures between the bulk phase and the SmE phase are observed at 149°C, the transition to SmA occurs at 220°C, and the final melting starts at 235°C. These phase transition temperatures are in quite good agreement with literature [9,10].

The phase transition at 149°C exhibits the vanishing of odd-numbered ($00l$) peaks from the bulk phase and a shift of the leftover even-numbered peaks to smaller q-values. The doubling of peak distances in q-space indicates a reduction of the interplanar distance by a factor of approximately two which means that the bilayer structure changes to a single-layer structure [14]. Please note that the molecular layer thickness corresponds approximately to the length of a single molecule which means that a single molecular sheet is
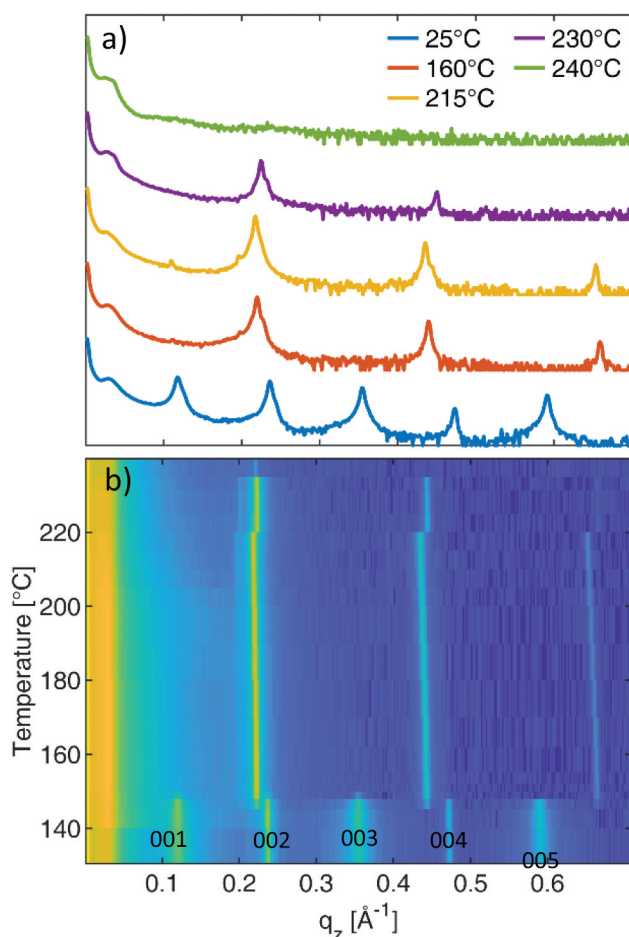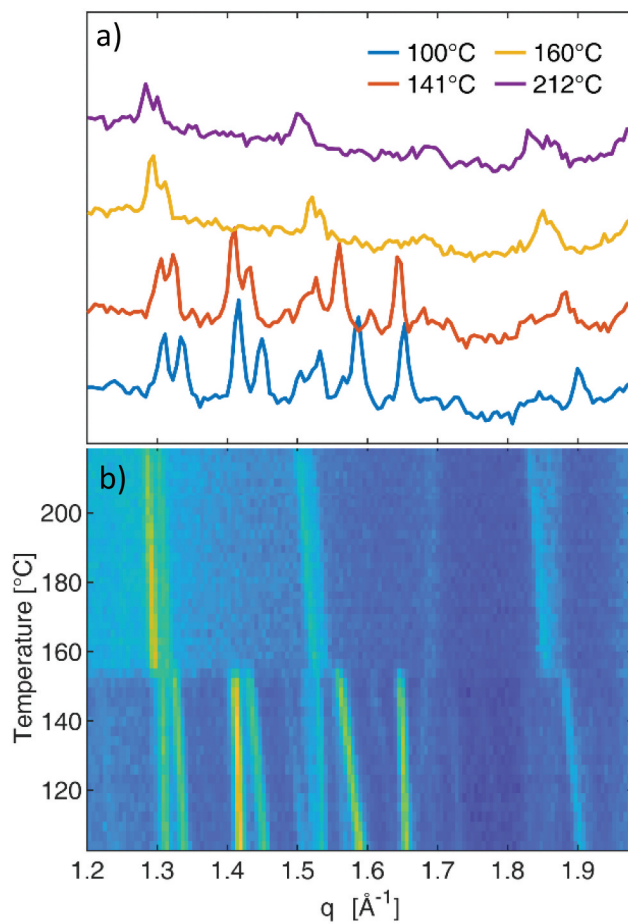
Figure 1. (Colour online) Specular X-ray diffraction of a Ph-BTBT -10 thin film as a function of temperature. Single scans of a film at selected temperatures (a) and a series of scans in the region between 120° and 240°C in a waterfall plot including the three-phase transitions: bulk phase/SmE at a temperature of 149°C, SmE/SmA at 220°C and SmA/isotropic state at 235°C (b).


Figure 2. (Colour online) Selected powder diffraction scans at different temperatures (a) and the complete series of X-ray powder diffraction scans in the temperature region between 100°C and 220°C illustrated in a waterfall plot (b). The phase transition from the bulk phase to the SmE phase is around 153°C.

composed of upright standing molecules. Therefore, we can conclude that the SmE phase as well as the SmA phase are formed by single sheets which are stacked upright onto each other parallel to the substrate surface.

Figure 2 shows a series of diffraction patterns as a function of temperature measured on a powder sample at higher values of q. Selected diffraction patterns are depicted in Figure 2(a), while a waterfall plot in a selected temperature range is given in Figure 2(b). A clear phase transition is visible at 153°C, a temperature slightly larger than observed at thin films. A continuous shift of the peak pattern is visible also before and after the phase transition due to thermal expansion. To study the evolution of the lattice constants as a function of temperature, the exact peak positions of all observed peaks of the bulk phase ($T < 153$°C) were determined (namely *00l, 010, 011, 100, 101, 110, 111, 020, 021, 120, 012, 102, 112*). The lattice constants *a, b, c* and the monoclinic angle *ß*

were determined as a function of temperature; the result is depicted in Figure 3. Within the bulk structure (temperature range from 60 to 153°C) the lattice constants *a* and *c* do not change significantly, but the lattice constant *b* increases and the monoclinic angle *ß* decreases.

The diffraction pattern at elevated temperatures ($T > 153$°C) is characteristic for a SmE phase with dominant peaks at 1.29, 1.52 and 1.85 Å^{-1} [27,28]. The refinement of the unit cell parameters after the phase transition resulted in a monoclinic angle very close to 90°, independent of temperature. An orthorhombic unit cell was concluded, a result which is comparable to other SmE phases [29–31].

At the transition temperature of 153°C, a clear shift in the lattice constants *b, c* and *ß* is observed, while a roughly continuous behaviour is observed for the lattice constant *a*. The volume of the crystallographic unit cell changes discontinuously from 2488.1 Å^3 (corresponding to 622 Å^3 per molecule) for the bulk crystal phase to 1462.0 Å^3 (731 Å^3 per molecule) for the SmE phase.
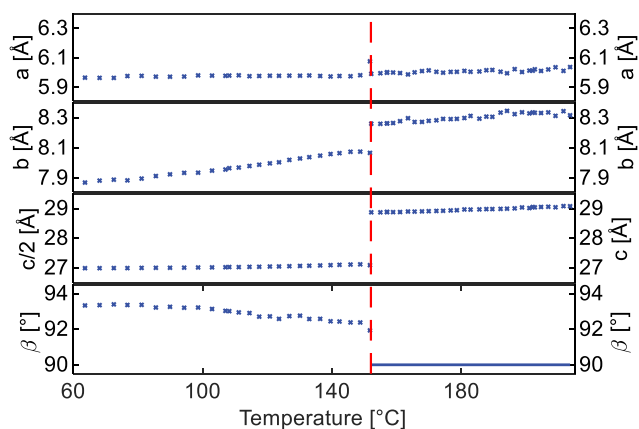
Figure 3. (Colour online) Lattice constants as a function of temperature of the bulk phase below a temperature of 153°C and of the smectic E phase between 153°C and 215°C. In case of the lattice constant *c*, the half of the lattice constant (*c*/2) is plotted for the bulk phase, while for the SmE phase the full length (*c*) is plotted.

A more detailed crystallographic study was performed by GIXD. In the first step the bulk structure of Ph-BTBT-10 was investigated for a drop casted film at room temperature. Figure 4(a) presents an experimental diffraction pattern taken at room temperature, and calculated peak positions are given by green spots and peak intensities by the area of the surrounding circles. The characteristic diffraction features of the bulk structure can be clearly identified as enhanced intensities along the *11 l, 02 l* and *12 l* rod. Moreover, characteristic packing features of the individual bulk structure of Ph-BTBT-10 can be identified by the enhanced intensities of the *112* and *115* peaks.

In a subsequent step, the SmE phase was investigated by GIXD at a temperature of 160°C. A spin coated thin film from a 5 g/l solution was used. The corresponding result is shown in Figure 4(b–d). A quite different diffraction pattern is observed in comparison to the bulk phase. Only a few diffraction peaks are observed, and they are arranged in two sequences at different q_{xy} values. Peaks along $q_z = 0$ (in-plane direction) reveal crystallographic order along the substrate surface, and these peaks represent crystallographic order within a single smectic plane. The peak series at $q_z \sim 0.22$ Å^{-1} reveals an onset of long-range (positional) order perpendicular to the substrate surface (*z*-direction). These peaks reveal an onset of three-dimensional crystallographic order due to stacking of smectic planes, which justifies the term *crystal smectic phase*. This diffraction pattern is in agreement with previous studies on SmE phases of other molecular materials showing a clear absence of peaks, corresponding to *10 l* and *01 l* peak series and six dominant peaks between $q = 1.3$ and 1.9 Å^{-1} (with Laue indices *110, 111, 020, 021, 120, 121*) [32]. Additionally, small intensities are found for the *200, 201* and *112* peaks (compare Figure 4(b–d)). The peak indexation is based on the results presented in Figure 3 using the following lattice constants of the
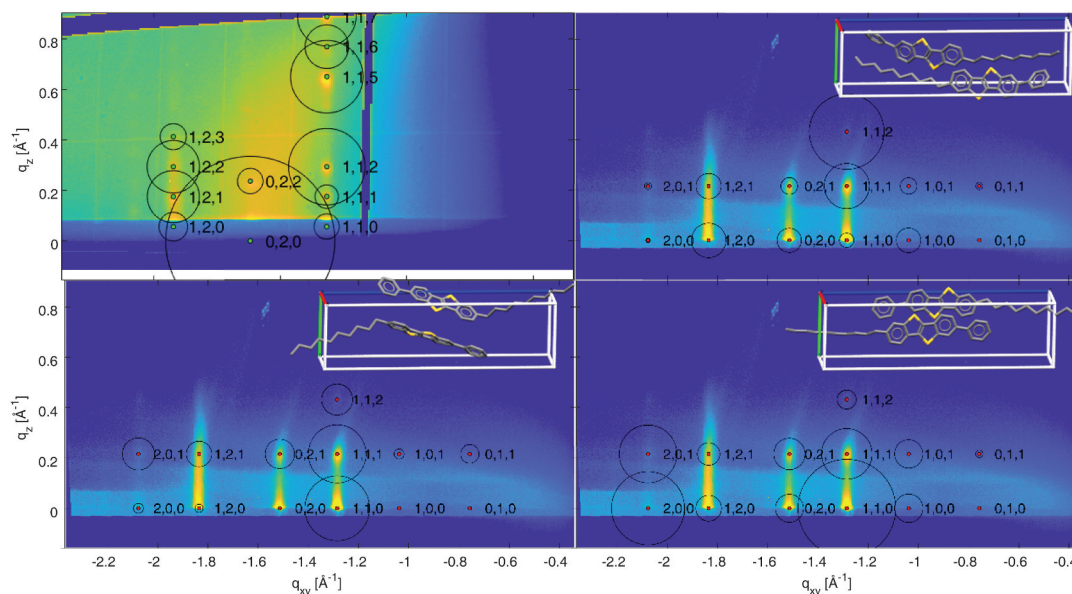
Figure 4. (Colour online) Grazing incidence X-ray diffraction pattern of Ph-BTBT-10 thin films at room temperature (a) and at a temperature of 160°C (b–d) with logarithmic scaling of the intensity. Additionally, calculated diffraction patterns are shown with points and circles representing positions and intensities of the calculated Bragg peaks, respectively. Different packing motifs are selected: the crystallographic bulk phase (a), SmE with mixed layers (b), SmE with nano-segregated layers possessing a herringbone arrangement (c) and a stacked arrangement (d). The insets give the different packing motifs relative to the crystallographic unit cell.
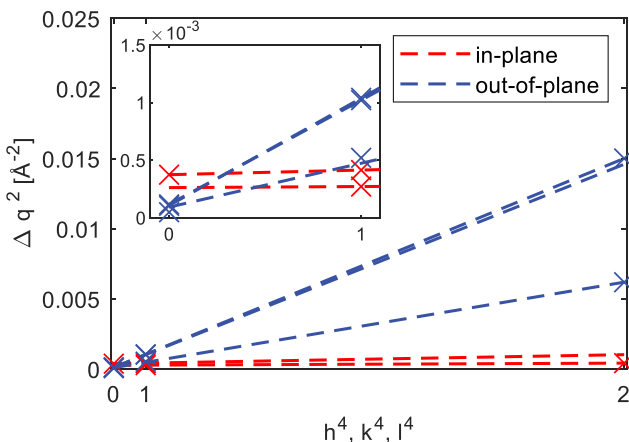
Figure 5. (Colour online) The square of in-plane peak width (Δq_{xy}^2) and of the out-of-plane peak width (Δq_z^2) plotted as a function of the fourth order of the Laue indices h,k,l. The linear regression is based on the paracrystalline model. The inset shows the range between $h,k,l = 0$ and $h,k,l = 1$.

orthorhombic unit cell at a temperature of 160°C: $a = 6.051$ Å, $b = 8.303$ Å and $c = 29.10$ Å.

Since only a limited number of peaks are observed, the long-range order of the molecules within the SmE phase is far from perfect. But in several cases higher-order diffraction peaks are observed so that an analysis in terms of a paracrystalline model can be applied [33]. Figure 5 shows fits of the paracrystalline model for five families of diffraction peaks (*11l, 02l* and *20l, h20, 1k0*) in terms of their in-plane peak widths Δq_{xy} and out-of-plane peak widths Δq_z, respectively, with a summary of the fit parameters in Table 1. Although the number of data points is limited (two or three), the complete set of data gives a clear trend for the two different directions. A crystallite size of about $D_z = 100$ Å and a paracrystallinity $g_z = 10\%$ is found for the out-of plane direction while values $D_{xy} = 50$ Å and $g_{xy} = 4\%$ is found for the in-plane direction. A g-value of less than 10% is classified as diffuse scattering from a disordered state [34].

In a next step, the molecular packing within the SmE phase is analysed. The sudden change of the lattice constant c at the phase transition temperature from 54.2 Å

for the bulk phase to 28.9 Å in the SmE phase (compare Figure 3) reflects the transition from a bilayer structure with *head-to-head* arrangement to a single-layer structure with *head-to-tail* arrangement. The transition can happen by lateral and vertical displacements of the molecule that avoid an energy demanding complete flip of the whole molecule [14,16]. As a consequence, the single-sheet structure is formed by antiparallel molecules with an alternating orientation of the aromatic cores giving the alkyl chains a parallel and antiparallel alignment to the $c^\star$-axis (perpendicular to the smectic layers).

The molecular dynamics simulations are based on the crystallographic unit cell containing two molecules. A number of different candidate packing motifs are found. Three of them show antiparallel molecules, which were selected for further considerations. Their respective molecular packings are shown as insets of Figure 4(b–d). In case of the first packing motif (denoted as mixed layers, Figure 4(b)), the individual layers are composed of blended decyl chains and aromatic units. In case of the second and third packing motif (denoted as nano-segregated), the structure shows a separation of the molecular parts into layers of aromatic units and layers of decyl chains. Within the nano-segregation further differentiation is found for the packing of the aromatic units (i) tilting relative to each other (herringbone arrangement, Figure 4(c)) or (ii) parallel stacking upon each other (stacked arrangement, Figure 4(d)). The respective crystallographic information files (cif – files) of these three packing motifs are given in the Supporting Information.

In a subsequent step, the three different packing motifs were used to calculate structure factors and compare them with experimental values. In the first step, R-factors were calculated for all observed Bragg peaks (compare Figure 4 (b–d)); the results are shown in Table 2. The largest R-factor is found for the mixed layer system, both nano-segregated structures show considerably smaller R-values. From this point of view, the mixed layer motif seems to be the least matching molecular packing within the SmE phase. However, it cannot be concluded which type of nano-segregated structure is present.

Our molecular dynamics simulations reveal that the three different packing motifs are associated with characteristic energies. Therefore, we use

Table 1. Crystallite sizes D_z and D_{xy} and degrees of paracrystallinity g_x and g_{xy} for five sets of diffraction peaks determined on the basis of the paracrystalline model for the *smectic E* phase of Ph-BTBT-10.

Laue indices	D_z (Å)	D_{xy} (Å)	g_z (%)	g_{xy} (%)
1 1 *l*	96.7	-	12.3	-
0 2 *l*	103	-	9.01	-
2 0 *l*	91.8	-	11.2	-
h 2 0	-	51.5	-	5.6
1 *k* 0	-	61.5	-	3.5

The respective values for the in-plane direction (along the smectic layers) and for the out-of-plane direction (across the smectic layers) are denoted by the subscripts *z* and *xy*, respectively.

Table 2. Comparison of the reliability factors for X-ray diffraction (*R*-factors) and of the total energies obtained from molecular dynamics calculations for the three different packing motifs.

Packing motif	R	Energy (%)
Mixed layer	1.53	130.7
Nano-segregated herringbone	0.67	100
Nano-segregated stacking	0.65	159.5

The energies are given relative to the lowest obtained energy.

these energies as a criterion for assigning a specific packing motif to the SmE phase. Since the obtained total energies are less meaningful, we decided to give fractional values relative to the lowest energy state (Table 2). Our calculation reveals that the herringbone packing is the lowest energy state and the difference with respect to the other two packings is comparably large. Please note that the higher energies for the two other packing motifs (mixed layer/nano-segregation with parallel stacking) is a consequence of squeezing the molecules into a given crystallographic unit cell. Therefore, the given energy values are not representative for a relaxed state of these two packing motifs.

Based on the comparison of the experimental and the calculated diffraction pattern together with energy considerations of the molecular dynamics simulations, we conclude that nano-segregation with herringbone packed aromatic units is present within the SmE phase of the molecule Ph-BTBT-10. The result that herringbone packing is present within the SmE phase is in accordance with the literature [26,28,34]. Please note that the negligible intensities of the *10 l* and *01 l* peaks in the experimental diffraction pattern (compare Figure 5(c)) is a characteristic feature of herringbone packing, frequently observed even for alkyl terminated conjugated molecules [17,35].

The analysis of the molecular packing for the nano-segregated herringbone structure in terms of molecular conformation reveals that a planar conformation of the aromatic unit is obtained. This can be expected since the antiparallel alignment of neighbouring the molecules causes that the phenyl and the BTBT units are next to each other. Thus, an integration of both units into an intermolecular herringbone arrangement makes a planarisation reasonable. A herringbone angle of 54° is obtained which is comparable with an angle of 50° observed for the bulk phase. The bent angle of the decyl side chain relative to the aromatic unit is 40°; this value is comparable to the 35° bent angle observed within the bulk phase.

Discussion

Asymmetric molecules which are composed of aromatic units and aliphatic chains show often combined SmE and SmA phases [27,29]. In the case of the molecule Ph-BTBT-10, we found a stacking distance of 28.1 Å for the SmA phase which is in quite good agreement with atomistic modelling by molecular dynamics [15].

Previous analysis of the molecular packing within the SmE phase of the molecule Ph-BTBT-10 was based on the transition from the bulk phase to the SmE phase. A bilayer structure showing *head-to-head* arrangements of the molecules is transferred to the SmE phase with a single-layer structure with *head-to-tail* arrangement. A mechanism for a defined transition from a *head-to-head* arrangement to a *head-to-tail* arrangement is possible by collective translational movement of the molecules [14,16].

Our approach with molecular dynamics simulation is based on the experimentally observed crystallographic unit cell of the SmE phase. Starting from random arrangements of the molecules, the system is reduced to the actual unit cell size. The obtained packing motifs are analysed in terms of energy and in accordance with the experimental diffraction pattern. Please note that the presented results consider rigid aromatic units and alkyl chains. Thermal movements, molecular disorder and displacement of the molecules (and atoms) are not included. It is stated in the literature that the alkyl chains are in a molten state within the SmE phase and the molecular packing is determined by the rigid character of the aromatic units [36,37]. We found that the packing of the aromatic units appears in herringbone arrangement. This is in agreement with the general expectation for the SmE phases as well as with recent findings [30,31,38].

Our results reveal that the molecular packing of the molecules is rather nano-segregated which means that the phenyl-BTBT units and the decyl units form separated layers within a molecular sheet. This is in agreement with the already published concepts for SmE [39,40]. The nano-segregated structure, together with the antiparallel alignment of the molecules, results in an interdigitation of the decyl chains originating from two aromatic layers of neighbouring layers. One further important result is related to the conformation of the molecule. It is found that the alkyl chains are bent relative to the aromatic core by an angle of 40°, which is in excellent agreement with the predicted angle of 43° for the 'bent-form' smectic phases [41]. Moreover, the appearance of clearly detectable *00l* Bragg peaks series from stacking of the smectic layers (in difference to a single *001* Bragg peak) supports the simple approach to assign a 'bent-form' smectic phase to the *crystal smectic E* phase [41].

Conclusion

Thin films of the molecule Ph-BTBT-10 are investigated in terms of their molecular packing as a function of temperature. A phase transition from the bulk state to a SmE phase and finally to a SmA phase is observed by XRD experiments. Sharp transitions from the bulk crystal phase to the SmE phase and further to SmA phase are observed at 149°C and 220°C, respectively. The transition to the SmE phase is associated with a change from

a monoclinic to an orthorhombic unit cell with a discontinuous change of the lattice constants. The available space of a single molecule increases substantially from 622 Å^3 in the bulk phase to 731 Å^3 in the SmE phase. Analysis of the peak width by a paracrystalline model reveals that the in-plane order is reduced (crystal size of 50 Å and 4% paracrystallinity) in comparison to the out-of plane order (100 Å / 10%). Based on the crystallographic lattice constants, obtained from GIXD analysis, molecular packing analysis was performed by molecular dynamics calculations. A comparison of calculated and experimental diffraction patterns, together with energy considerations, reveals nano-segregation of the decyl units from the aromatic unis, together with herringbone arrangements of the aromatic units. The specific conformation of the molecules with a defined bent angle between the aromatic units and the decyl chains reveals that the *crystal smectic E* phase of the molecule Ph-BTBT-10 is of 'bent-form' type.

Associated content

Crystallographic information files for the three considered different molecular packings. Structures formed by (i) sheets of blended decyl chains and aromatic units (mixed_layer.cif), sheets of nano-segregated decyl chains and aromatic units with (ii) herringbone arrangement of the aromatic units (nanoegregated_herringbone.cif) and (iii) with parallel stacking of the aromatic units (nano-segregated_stacking.cif).

Disclosure statement

No potential conflict of interest was reported by the author(s).

ORCID

Sebastian Hofer http://orcid.org/0000-0002-8958-6815
Wolfgang Bodlos http://orcid.org/0000-0002-6187-5260
Jiří Novák http://orcid.org/0000-0003-4664-746X
Luca Beverina http://orcid.org/0000-0002-6450-545X
Roland Resel http://orcid.org/0000-0003-0079-3525

References

[1] Ebata H, Izawa T, Miyazaki E, et al. Highly soluble [1]benzothieno[3,2-b]benzothiophene (BTBT) derivatives for high-performance, solution-processed organic field-effect transistors. J Am Chem Soc. 2007;129:15732–15733.

[2] Minemawari H, Yamada T, Matsui H, et al. Inkjet printing of single-crystal films. Nature. 2011;475:364–367.

[3] Izawa T, Miyazaki E, Takimiya K. Molecular ordering of high-performance soluble molecular semiconductors and re-evaluation of their field-effect transistor characteristics. Adv Mater. 2008;20:3388–3392.

[4] Dohr M, Werzer O, Shen Q, et al. Dynamics of monolayer-island transitions in 2,7-dioctyl- benzothienobenzthiophene thin films. ChemPhysChem. 2013;14:2554–2559.

[5] Spreitzer H, Kaufmann B, Ruzié C, et al. Alkyl chain assisted thin film growth of 2,7-dioctyloxy-benzothienobenzothiophene. J Mater Chem C. 2019;7:8477–8484.

[6] Lyu L, Niu D, Xie H, et al. The correlations of the electronic structure and film growth of 2,7-diocty[1]benzothieno[3,2-: B] benzothiophene (C8-BTBT) on SiO2. Phys Chem Chem Phys. 2017;19:1669–1676.

[7] Iino H, Hanna JI. Availability of liquid crystallinity in solution processing for polycrystalline thin films. Adv Mater. 2011;23:1748–1751.

[8] Iino H, Hanna JI. Liquid crystalline organic semiconductors for organic transistor applications. Polym J. 2017;49:23–30.

[9] Iino H, Usui T, Hanna JI. Liquid crystals for organic thin-film transistors. Nat Commun. 2015;6:6828.

[10] Inoue S, Minemawari H, Tsutsumi J, et al. Effects of substituted alkyl chain length on solution-processable layered organic semiconductor crystals. Chem Mater. 2015;27:3809–3812.

[11] Wu H, Iino H, Hanna JI. Thermally induced bilayered crystals in a solution-processed polycrystalline thin film of phenylterthiophene-based monoalkyl smectic liquid crystals and their effect on FET mobility. RSC Adv. 2017;7:56586–56593.

[12] Minemawari H, Tsutsumi J, Inoue S, et al. Crystal structure of asymmetric organic semiconductor 7-decyl-2-phenyl[1]benzothieno[3,2- b][1]benzothiophene. Appl Phys Express. 2014;7:2–5.

[13] Iino H, Hanna JI. Liquid crystal and crystal structures of a phenyl-benzothienobenzothiophene derivative. Mol Cryst Liq Cryst. 2017;647:37–43.

[14] Yoneya M. Monolayer crystal structure of the organic semiconductor 7-Decyl-2-phenyl[1]benzothieno[3,2- b][1]benzothiophene. J Phys Chem C. 2018;122:22225–22231.

[15] Baggioli A, Casalegno M, Raos G, et al. Atomistic simulation of phase transitions and charge mobility for the organic semiconductor Ph-BTBT-C10. Chem Mater. 2019;31:7092–7103.

[16] Yoneya M. Monolayer crystal structure of the organic semiconductor 7-decyl-2-phenyl[1]benzothieno[3,2-b][1]benzothiophene, revisited. Jpn J Appl Phys. 2020;59: 090909.

[17] Lercher C, Röthel C, Roscioni OM, et al. Polymorphism of dioctyl-terthiophene within thin films: the role of the first monolayer. Chem Phys Lett. 2015;630:12–17.

[18] Pithan L, Nabok D, Cocchi C, et al. Molecular structure of the substrate-induced thin-film phase of tetracene. J Chem Phys. 2018;149:149.

[19] Jones AOF, Röthel C, Lassnig R, et al. Solution of an elusive pigment crystal structure from a thin film: a combined X-ray diffraction and computational study. CrystEngComm. 2017;19:1902–1911.

[20] Sanzone A, Mattiello S, Garavaglia GM, et al. Efficient synthesis of organic semiconductors by Suzuki-Miyaura coupling in an aromatic micellar medium. Green Chem. 2019;21:4400–4405.

[21] Resel R, Tamas E, Sonderegger B, et al. A heating stage up to 1173 K for X-ray diffraction studies in the whole orientation space. J Appl Crystallogr. 2003;36:80–85.

[22] Fumagalli E, Campione M, Raimondo L, et al. Grazing-incidence X-ray diffraction study of rubrene epitaxial thin films. J Synchrotron Radiat. 2012;19:682–687.

[23] Anton Paar GmbH DHS1100: a new high-temperature attachment for materials science in the whole orientation space. J Appl Crystallogr. 2007;40:202.

[24] Schrode B, Pachmajer S, Dohr M, et al. GIDVis: a comprehensive software tool for geometry-independent grazing-incidence X-ray diffraction data analysis and pole-figure calculations. J Appl Crystallogr. 2019;52:683–689.

[25] Plimpton S. Fast parallel algorithms for short-range molecular dynamics. J Comput Phys [Internet]. 1995;117:1–19. Available from: http://www.cs.sandia.gov/sjplimp/main.html

[26] Brooks BR, Brooks C, Mackerell AD, et al. CHARMM: molecular dynamics simulation package. J Comput Chem. 2009;30:1545–1614.

[27] Pensec S, Tournilhac FG, Bassoul P. Structure of the mesophases formed by a perfluoroalkyl/biphenyl compound. Amphiphilic and steric effects. J Phys II. 1996;6:1597–1605.

[28] Jasiurkowska M, Budziak A, Czub J, et al. X-ray studies on the crystalline e phase of the 4-n-alkyl-4′- isothiocyanatobiphenyl homologous series (nBT, n = 2–10). Liq Cryst. 2008;35:513–518.

[29] Diele S, Tosch S, Mahnke S, et al. Structure and packing in smectic E and smectic A phases in the series of 4-n-Alkyloxy-4′-alkanoylbiphenyls. Cryst Res Technol. 1991;26:809–817.

[30] Voronov VP, Muratov AR, Sulyanov SN, et al. Interplay between various crystalline and hexatic-B phases in 75OBC liquid crystal: X-ray diffraction and calorimetry study. Liq Cryst. 2020;47:1366–1378.

[31] Schulz F, Ehni P, Wank B, et al. Alkoxy-bromo-azulenes displaying ambient temperature smectic E-phases. Liq Cryst. 2020;1–12.

[32] Seddon JM. Structural studies of liquid crystals by X-ray diffraction. Handb Liq Cryst. 1998;1:635–679.

[33] Hosemann R. Crystalline and paracrystalline order in high polymers. J Appl Phys. 1963;34:25–41.

[34] Bonart R, Hosemann R, McCullough RL. The influence of particle size and distortions upon the X-ray diffraction patterns of polymers. Polymer. 1963;4:199–211.

[35] Jones AOF, Chattopadhyay B, Geerts YH, et al. Substrate-induced and thin-film phases: polymorphism of organic materials on surfaces. Adv Funct Mater. 2016;26:2233–2255.

[36] Yamamura Y, Adachi T, Miyazawa T, et al. Calorimetric and spectroscopic evidence of chain-melting in smectic e and smectic a phases of 4-alkyl-4′-isothiocyanatobiphenyl (n TCB). J Phys Chem B. 2012;116:9255–9260.

[37] Horiuchi K, Yamamura Y, Pełka R, et al. Entropic contribution of flexible terminals to mesophase formation revealed by thermodynamic analysis of 4-Alkyl-4′-isothiocyanatobiphenyl (n TCB). J Phys Chem B. 2010;114:4870–4875.

[38] Barón M, Noël C, Shibaev VP, et al. Definitions of basic terms relating to low-molar-mass and polymer liquid crystals (IUPAC recommendations 2001). Pure Appl Chem. 2001;73:845–895.

[39] Saito K, Miyazawa T, Fujiwara A, et al. Reassessment of structure of smectic phases: nano-segregation in smectic E phase in 4-n-alkyl-4-isothiocyanato-1,1-biphenyls4-n-alkyl-4′-isothiocyanato-1,1′-biphenyls. J Chem Phys. 2013;139:114902.

[40] Miyazawa T, Yamamura Y, Hishida M, et al. Revisiting smectic E structure through swollen smectic E phase in binary system of 4-nonyl-4′-isothiocyanatobiphenyl (9TCB) and n-nonane. J Phys Chem B. 2013;117:8293–8299.

[41] Yamamura Y, Murakoshi T, Hishida M, et al. Examination of molecular packing in orthogonal smectic liquid crystal phases: a guide for molecular design of functional smectic phases. Phys Chem Chem Phys. 2017;19:25518–25526.